

Properties of Grooved Dayem Bridge based $\text{YBa}_2\text{Cu}_3\text{O}_{7-\delta}$ Superconducting Quantum Interference Devices and Magnetometers

E. Trbaldo,¹ S. Ruffieux,¹ E. Andersson,¹ R. Arpaia,^{1,2} D. Montemurro,^{1, a)} J.F. Schneiderman,³ A. Kalaboukhov,¹ D. Winkler,¹ F. Lombardi,¹ and T. Bauch^{1, b)}

¹⁾*Quantum Device Physics Laboratory, Department of Microtechnology and Nanoscience, Chalmers University of Technology, SE-41296 Göteborg, Sweden*

²⁾*Dipartimento di Fisica, Politecnico di Milano, Piazza Leonardo da Vinci 32, I-20133 Milano, Italy*

³⁾*MedTech West and the Institute for Neuroscience and Physiology, Sahlgrenska Academy, University of Gothenburg, SE-40530 Göteborg, Sweden*

(Dated: 24 January 2020)

The transport properties of a $\text{YBa}_2\text{Cu}_3\text{O}_{7-\delta}$ superconducting quantum interference device (SQUID) based on grooved Dayem bridge weak links are studied as a function of temperature: at high temperatures ($60 \text{ K} < T < T_c = 89 \text{ K}$) the weak links show properties similar to SNS junctions, while at temperatures below 60 K the weak links behave like short Dayem bridges. Using these devices, we have fabricated SQUID magnetometers with galvanically coupled in-plane pick-up loops: at $T = 77 \text{ K}$, magnetic field white noise levels as low as $63 \text{ fT}/\sqrt{\text{Hz}}$ have been achieved.

^{a)}Present address: Dipartimento di Fisica, Università di Napoli Federico II, Via Cinthia, I-80126 Napoli, Italy

^{b)}Electronic mail: thilo.bauch@chalmers.se

One of the most prominent applications of superconducting materials is the superconducting quantum interference device (SQUID)¹. SQUIDs are used in geophysical surveys and mining, non-destructive structure evaluation, scanning SQUID microscopy, and biomagnetic diagnostics (magnetoencephalography, magnetocardiography, etc)²⁻⁵. State of the art SQUIDs are based on low critical temperature superconductors (LTS)⁶ typically requiring expensive and scarce liquid helium for their operation. High critical temperature superconductor (HTS) based SQUIDs, instead, can be operated at liquid nitrogen temperatures. The use of cheap and abundant liquid nitrogen furthermore simplifies the cryogenic requirements in terms of cooling and thermal insulation as compared to LTS-based systems. The realization of HTS Josephson junctions, the key ingredient of a SQUID, has been a topic of intense research during the last three decades⁷⁻¹¹. The state-of-the-art HTS SQUIDs operating near 77 K typically use either bicrystal or step edge grain boundary Josephson junctions.¹²⁻¹⁶ However, bicrystal junctions need to be placed at the grain boundary line, while step edge junctions require more than one lithography step¹⁷ and several epitaxial thin film depositions.¹² The recent development of the YBCO grooved Dayem bridge (GDB) made it possible to realize SQUID magnetometers with magnetic field noise values at 77 K comparable to the best single layer devices.¹⁸ In contrast to grain boundary JJs, GDBs can be defined anywhere on the chip and oriented at will within the film plane. Moreover, the bridge and weak link inside it are realized during a single lithography process. However, the nature of the GDB weak link determining its transport properties has not been explored yet.

In this letter we present a study of GDB-based SQUID properties as a function of temperature. From the temperature dependence of these properties, we conclude that the GDB is governed by superconductor-normal conductor-superconductor (SNS) like behaviour at $T > 60$ K, whereas at lower temperatures the weak link is better described by an SS'S type of weak link, where S' describes a superconducting constriction. By coupling a GDB-based SQUID galvanically to a $9 \text{ mm} \times 8.7 \text{ mm}$ pick-up loop on a $10 \text{ mm} \times 10 \text{ mm}$ substrate we achieve a magnetic field sensitivity as low as $63 \text{ fT}/\sqrt{\text{Hz}}$ at 77 K.

The SQUIDs are fabricated by first depositing a 50 nm thick $\text{YBa}_2\text{Cu}_3\text{O}_{7-\delta}$ (YBCO) film on a (001) oriented SrTiO_3 substrate by pulsed laser deposition (PLD). The lateral size of the substrate is $10 \text{ mm} \times 10 \text{ mm}$ which allows accommodation of a pick-up loop, and thus an effective area, that is significantly larger as compared to our previous work.¹⁸ The deposition conditions have been tuned so that the YBCO film is close to optimally doped (critical temperature $T_c \simeq 89.0$ K) and c -axis oriented.^{19,20} An amorphous carbon film, with thickness $t_C = 100$ nm, is deposited by

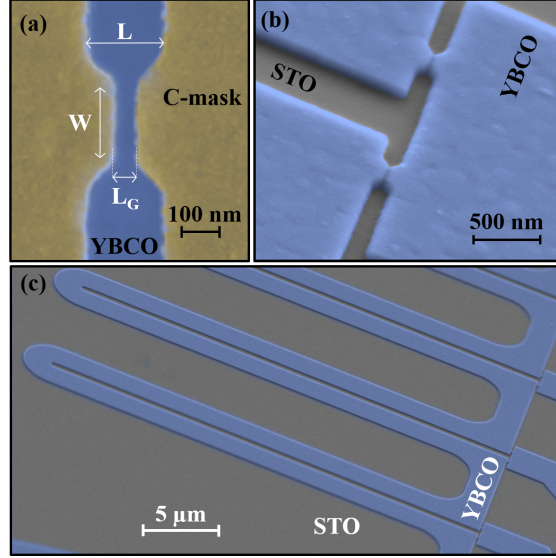


FIG. 1. (a) Example of a carbon mask for the realization of a GDB prior to Ar^+ ion milling. The mask dimensions are $W = 200$ nm, $L = 150$ nm and $L_G = 50$ nm. (b) SEM image of two GDBs patterned in a SQUID loop. (c) SEM image of a series of SQUID loops.

PLD on top of the YBCO film, which is subsequently patterned by electron beam lithography (EBL) and oxygen plasma reactive ion etching. The pattern of the carbon mask is transferred to the YBCO film using low voltage (300 eV) Ar^+ ion milling. The Ar^+ ion milling parameters have been tuned to minimize damage to the superconducting nanostructures.^{21–23}

A Grooved Dayem Bridge (GDB) is obtained by designing a gap in the carbon mask, along the whole width of a short nanowire (Dayem bridge), with a typical gap length $L_G = 50$ nm, see Fig.1(a). The etching rate during Ar^+ ion milling of the material inside the nano-gap is decreased compared to the rest of the sample, when $t_C/L_G \gtrsim 2$.^{18,24} In this regime, the increased re-deposition rate inside the nano-gap leads to a reduced effective etching rate. The final result of the Ar^+ ion milling is a nano-bridge with width $W = 200$ nm and length $L = 150$ nm and with a groove etched in the center, which acts as a weak link (see Fig.1(b)). The whole mask design (nanostructures and pick-up loop) is defined in a single EBL step, avoiding alignment errors, which are common in nano-fabrication processes involving several lithography steps.^{25,26} The single step of Ar^+ ion milling required to define the device simplifies the fabrication process and minimizes the detrimental effect of Ar^+ ion milling to the YBCO nanostructures. The SQUID loop has a hairpin design²⁷ (see Fig. 1(c)) with hair pin slit length, l_{slit} , ranging from 8 to 36 μm , slit width of 500 nm, and line width of 2 μm . The GDBs act as the SQUID weak links (Fig. 1(b)) where the groove locally

reduces the I_c of the nano-bridge. The electric and magnetic parameters of the 4 SQUIDs studied in this work are summarized in Table I.

The sensitivity of a SQUID magnetometer is limited by its magnetic flux noise $S_{\Phi}^{1/2}$ (1/f and white), and its effective area, A_{eff} . The minimal intrinsic flux noise of a SQUID can be achieved for a screening parameter²⁸ $\beta_L = I_c L_{\text{SQ}} / \Phi_0$ close to 1. Here, I_c is the SQUID critical current, L_{SQ} is the total inductance of the SQUID (including hair pin loop inductance L_c and the parasitic kinetic inductance of the GDB L_k), and Φ_0 the superconducting flux quantum. The large critical current density, $j_c \simeq 3 \cdot 10^6 \text{ A/cm}^2$, at 77 K of bare YBCO Dayem bridges^{21,29}, together with the parasitic kinetic inductance of a Dayem bridge of thickness t and width w , $L_k = L\mu_0\lambda^2/wt$, sets a lower bound for the screening factor, $2I_c L_k / \Phi_0 = 4j_c L\mu_0\lambda^2 / \Phi_0$ on the order of 1-3 at 77 K for a typical bridge length $L = 150 \text{ nm}$.²⁹ Here λ , and μ_0 are the London penetration depth, and the vacuum permeability, respectively. Instead, for SQUIDs implementing GDBs, the contribution of the parasitic kinetic inductance to β_L is well below 0.3 at $T = 77 \text{ K}$, because the critical current density, I_c^G / wt , with I_c^G the critical current of the GDB, is at least a factor of 10 lower than that of bare Dayem bridges.¹⁸ This furthermore allows for sizable SQUID hair pin loops, which increases the effective area of the magnetometer and minimizes the resulting magnetic field noise as will be discussed below.

The amplifier input voltage noise $S_{V,a}^{1/2}$ contribution to the total white flux noise should moreover be minimized. This contribution is given by $S_{\Phi,a}^{1/2} = S_{V,a}^{1/2} / V_{\Phi}$, where $V_{\Phi} = \max(\delta V / \delta \Phi) \simeq \pi \Delta V_{\text{max}} / \Phi_0$ is the SQUID voltage-to-flux transfer function. ΔV_{max} is the maximum voltage modulation depth in response to an externally applied magnetic flux (see Fig. 2). ΔV_{max} can be approximated by $\Delta I_c \delta R$, where ΔI_c and δR are the critical current modulation depth and the differential resistance at the optimal bias current working point (i.e., where $\Delta V = \Delta V_{\text{max}}$), respectively. Therefore, a large value of δR is desirable in order to minimize the contribution of the amplifier voltage input noise to the total flux noise.

In Fig. 2(a) we show the current voltage characteristics of SQUID SQ2 (see Table I for details) measured at $T = 77 \text{ K}$ for two different applied magnetic flux values. The shape of the current voltage characteristics resembles that of a resistively shunted junction (RSJ). The voltage modulations of SQUID SQ2 as a function of applied magnetic flux are shown in the inset of Fig. 2(a). Here each curve corresponds to an increment of bias current, I_b , by $2 \mu\text{A}$. From this measurement one can extract the voltage modulation depth as a function of the bias current, which is shown in Fig. 2(b). From the maximum voltage modulation depth $\Delta V_{\text{max}} = 16.5 \mu\text{V}$ we obtain for the trans-

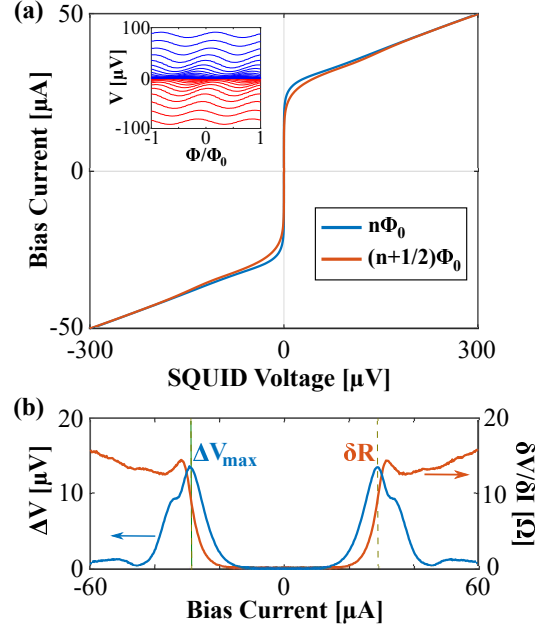


FIG. 2. (a) Current voltage characteristic of SQUID SQ2 at $T = 77$ K for two different values of applied magnetic flux. The inset shows the SQUID voltage modulations as a function of applied magnetic flux for various fixed bias currents with current step size $2 \mu\text{A}$ (b) Differential resistance $\delta V / \delta I$ for $n\Phi_0$ and voltage modulation depth ΔV as a function of applied bias current I_b . The value δR is indicated as the differential resistance at the optimal working point where V_Φ is maximized ($\Delta V = \Delta V_{\max}$).

fer function $V_\Phi = 52 \mu\text{V} / \Phi_0$ at $T = 77$ K. This is a net improvement compared to nanowire-based SQUIDs with similar SQUID loop size l_{slit}^{27} , which is attributed to the increased differential resistance and reduced parasitic inductance of GDBs as compared to bare nanowires. As will be shown below, this results in lower magnetic flux and field noise as well. The values of ΔV_{\max} measured at $T = 77$ K for the other SQUIDs are summarized in Table I.

In Fig. 3 (a), we show the maximum modulation depth ΔV_{\max} of SQUID SQ0 as a function of temperature T . In the temperature range between 10 K and 20 K, $\Delta V_{\max}(T)$ decreases rapidly with temperature. Increasing the temperature above 20 K up to $T \sim 55$ K causes ΔV_{\max} to further decrease slightly. For temperatures above 55 K we observe an increase of ΔV_{\max} up to $T = 65$ K above which the maximum voltage modulation depth goes to zero when reaching the critical temperature of the GDBs, $T_c^{\text{GDB}} \simeq 84$ K.

The non-monotonic behavior of $\Delta V_{\max}(T)$ can be understood from the temperature dependence of the critical current modulation depth ΔI_c and the differential resistance δR at the optimal working point, which are shown in Fig. 3(b). The critical current modulation depth decreases with

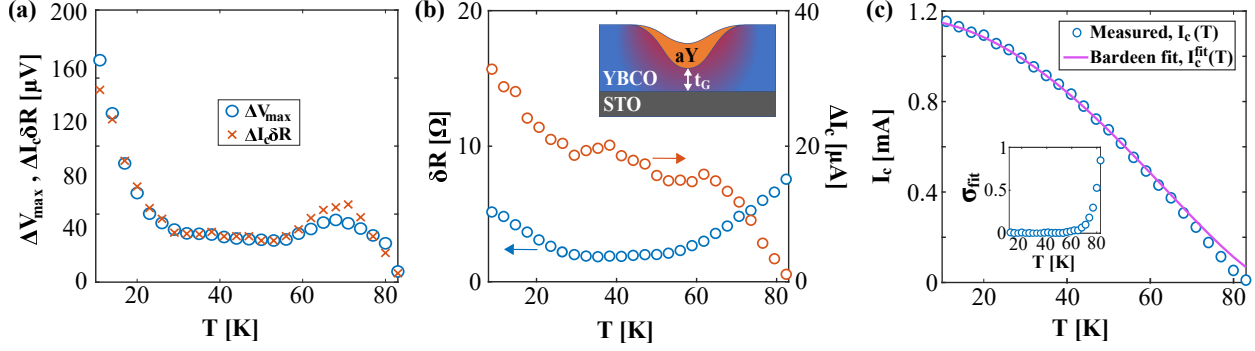


FIG. 3. (a) The voltage modulation at working point ΔV_{\max} (circles), obtained as the maximum of the measured ΔV , is compared as a function of the temperature to the product $\Delta I_c \delta R$ (crosses). (b) Differential resistance at the working point δR and critical current modulation depth ΔI_c vs. T . The inset shows a schematic cross section of a GDB. t_G is the thickness of the superconducting YBCO in the groove, while aY represents the amorphous YBCO layer re-deposited during Ar^+ ion milling. (c) Measured critical current versus temperature, I_c (open symbols), compared to the Bardeen fit, I_c^{fit} (solid line). Inset show the deviation, σ_{fit} , of the measured critical current from the fit as $\sigma_{\text{fit}} = (I_c^{\text{fit}} - I_c)/I_c^{\text{fit}}$

increasing temperature whereas the differential resistance first decreases with temperature until it increases again for temperatures above $T = 55$ K. The increase of the differential resistance with temperature is a typical feature of an SNS-like junction. The product $\Delta I_c \delta R$, shown in comparison with $\Delta V_{\max}(T)$ in Fig. 3(a) (crosses), reproduces nicely the maximum value of measured voltage modulation depth.

In Fig. 3 (c) we show the critical current I_c of device SQ0 as a function of temperature (blue circles). The solid line is the Bardeen expression for the depairing critical current of superconducting nanowires^{21,30}: $I_c^{\text{fit}}(T) \propto (1 - (T/T_c)^2)^{3/2}$. Here we used $T_c = 89$ K, the critical temperature of the YBCO film. In our previous work²¹ we have shown that the Bardeen expression properly reproduces the critical current of YBCO nanowires in the full temperature regime. The fact that the critical current of our GDBs can be well fitted by the Bardeen expression for temperatures below $T \simeq 60$ K suggests that the GDBs behave like short Dayem bridges at low temperatures. Here the length of the bridge is approximately given by the GDB gap length ($L_G = 50$ nm) and the thickness is given by the thickness of the remaining superconducting film, t_G , inside the gap buried under the redeposited amorphous YBCO¹⁸ (see inset Fig. 3(b)). From the typical critical current density of thin YBCO Dayem bridges³¹ $j_c \simeq 2 \times 10^7$ A/cm² at 4.2 K, we therefore obtain for the thickness of the superconducting constriction in the GDB $t_G \simeq 15$ nm.

For $T > 60$ K the measured critical current, $I_c(T)$, clearly departs from the temperature dependence of a bare Dayem bridge predicted by the Bardeen expression, $I_c^{\text{fit}}(T)$. A possible explanation is the weakening of superconductivity in the constriction of the GDB for T approaching $T_c^{\text{GDB}} \simeq 84$ K, which could also explain the increase of the differential resistance above $T = 60$ K. Indeed, in thin ($t \leq 30$ nm) YBCO films, a clear broadening of the superconducting transition in resistance vs temperature measurements has been observed³¹. This broadening can be attributed to a Kosterlitz-Thouless vortex-antivortex pair dissociation transition close to the T_c of the film^{32,33}. Alternative explanations include thermal activation of vortex-antivortex pairs or vortices overcoming the Bean-Livingston edge barrier.³⁴

The magnetic field noise of SQUID-based magnetometers can be obtained from the flux noise as $S_B^{1/2} = S_\Phi^{1/2} / A_{\text{eff}}$, where $A_{\text{eff}} = \Phi / B_a$ (here Φ and B_a are the magnetic flux through the SQUID loop and the externally applied magnetic field, respectively). Due to their small size, bare SQUIDs have extremely small effective areas A_{eff} , resulting in rather large values for $S_B^{1/2}$. This is a problem that is common to all SQUIDs, but particularly acute for nanoSQUIDs. To improve the magnetic field sensitivity, SQUIDs can be coupled to a much larger pick-up loop.⁸ We galvanically coupled 32 SQUIDs to a single pick-up loop, which is integrated directly in the EBL design of the sample, without additional fabrication steps. A schematic of the pick-up loop is shown in the inset of Fig. 4. The pick-up loop has lateral sizes of 8.7 mmx9 mm and line width of 2 mm.

An externally applied magnetic field results in a screening current circulating the loop $I_S \propto B_a$ which results in a phase difference between the weak links $\Delta\phi \propto I_S L_c 2\pi / \Phi_0$. L_c is the SQUID hairpin loop inductance and represents the coupling inductance between SQUID and pick-up loop. This coupling determines the effective area as³⁵ $A_{\text{eff}} = A_{\text{NS}} + A_{\text{eff}}^{\text{pl}} L_c / L_{\text{loop}}$, where A_{NS} and $A_{\text{eff}}^{\text{pl}}$ are the effective areas of the SQUID and pick-up loop, respectively. L_{loop} is the inductance of the pick-up loop. To increase A_{eff} , one needs to increase the coupling by increasing L_c . Since a higher SQUID inductance increases the screening factor β_L , in order to obtain the lowest $S_B^{1/2}$, the value of L_c needs to be optimized. The coupling inductance values of three SQUIDs were measured using a current injection scheme.³⁶ The injection current modulates the phase difference between the two GDBs. From the modulation period of the critical current ΔI_{mod} one can extract the inductance of the hairpin loop $L_c = \Phi_0 / \Delta I_{\text{mod}}$. In Table I we summarize the values of the coupling inductance of the various SQUIDs measured at $T = 77$ K.

The magnetic field sensitivity of three different devices were measured at $T = 77$ K in a magnetically shielded room. A commercial Magnicon SEL-1 dc-SQUID electronics³⁷ operated in flux-

TABLE I. Summary of the geometrical (gap length, L_G , and width W , SQUID loop slit length l_{slit} and effective area A_{eff}) and electrical properties of different SQUID-based magnetometers measured at $T = 77$ K.

| | L_G | W | l_{slit} | I_c | L_c | β_L | ΔV_{max} | A_{eff} | S_Φ | S_B |
|-----|-------|------|-------------------|-------------------|-------|-----------|-------------------------|-------------------|--|--|
| | [nm] | [nm] | [μm] | [μA] | [pH] | | [μV] | [mm^2] | [$\frac{\mu\Phi_0}{\sqrt{\text{Hz}}}$] | [$\frac{\text{fT}}{\sqrt{\text{Hz}}}$] |
| SQ0 | 40 | 150 | 8 | 92 | - | - | 30 | - | - | - |
| SQ1 | 50 | 200 | 16 | 15 | 48.5 | 0.3 | 39 | 0.15 | 6 | 85 |
| SQ2 | 50 | 200 | 30 | 30 | 103 | 1.5 | 16.5 | 0.35 | 10.6 | 63 |
| SQ3 | 50 | 200 | 30 | 16 | 103 | 0.8 | 18.7 | 0.35 | 11 | 67 |

locked loop and bias reversal (40 kHz) mode was used to measure the magnetic flux noise. From the measured magnetic flux noise $S_\Phi^{1/2}$, the magnetic field noise is calculated as $S_B^{1/2} = S_\Phi^{1/2}/A_{\text{eff}}$. Here the effective area was separately measured via responsivity measurements using a calibrated Helmholtz coil.³⁸ In Table I we summarize the magnetic noise properties of three different SQUID magnetometers. Devices SQ2 and SQ3 were fabricated on the same chip sharing the same pick-up loop, whereas SQ1 was realized on a different chip. The best performance in terms of voltage modulations and flux noise are achieved on device SQ1. This would be expected given the shorter l_{slit} and, consequently, smaller L_c . However, this also results in a smaller A_{eff} , compared to SQ2 and SQ3, due to reduced coupling. Indeed, devices SQ2 and SQ3, which have larger l_{slit} , show better coupling but at the cost of a reduced ΔV . Nevertheless, the V_Φ of SQ2 and SQ3 results in $S_\Phi^{1/2}$ comparable to state-of-the-art YBCO SQUIDs ($S_\Phi^{1/2} = 2.6 - 10 \mu\Phi_0/\sqrt{\text{Hz}}$, achieved in devices based on grain boundary junctions^{12-14,38-40}). The lowest magnetic noise spectral density was achieved for SQ2 and is shown in Fig. 4. The $1/f$ knee is below 3 Hz and the white magnetic field noise is around 63 fT/ $\sqrt{\text{Hz}}$. This result is almost a factor 2 lower than that which was previously obtained with GDB weak links¹⁸ and represents the lowest field noise achieved in SQUID magnetometers implementing Dayem bridge based weak links. Moreover, the measured magnetic field noise is comparable with the lowest reported field noise values achieved with single-layer grain boundary-based SQUIDs galvanically coupled to a pick-up loop made on 10 mm \times 10 mm substrates^{12,14,16,38,41}, $S_B^{1/2} = 30 - 50 \text{ fT}/\sqrt{\text{Hz}}$.

In conclusion, we have studied the temperature dependence of GDB based SQUIDs. At low temperatures, the GDBs behave like short and thin Dayem bridges, whereas at temperatures above

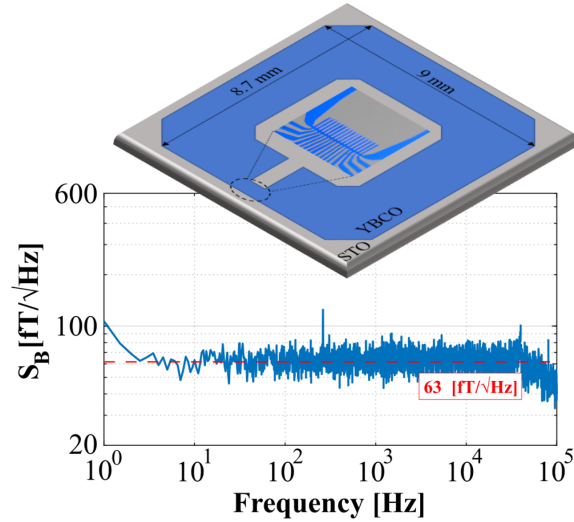


FIG. 4. Magnetic field noise spectrum of SQ2. The inset shows the design of the pick-up loop. In the center of the loop is shown an SEM figure of a series of SQUID loops (comb-like structure) which are coupled on the sides to the pick-up loop

60 K the fluctuation-driven suppression of superconductivity in the constriction of the GDB causes the weak link to behave like an SNS junction. This results in a local maximum in the temperature dependence of the transfer function around 65 K. Magnetic field noise as low as $63 \text{ fT}/\sqrt{\text{Hz}}$ at $T = 77 \text{ K}$ has been obtained for GDB based magnetometers galvanically coupled to an in-plane pick-up loop. Such low values makes these devices an attractive candidate for magnetoencephalography application, possibly outperforming their LTS counterpart.⁴²

ACKNOWLEDGMENTS

This work was been supported in part by the Knut and Alice Wallenberg Foundation (KAW) and in part by the Swedish Research Council (VR). This project has received funding from the ATTRACT project funded by the EC under Grant Agreement 777222. R.A. is supported by the Swedish Research Council (VR) under the project 2017-00382. This work was performed in part at Myfab Chalmers.

REFERENCES

- ¹H. Weinstock, *SQUID sensors: fundamentals, fabrication and applications*, Vol. 329 (Springer Science & Business Media, 2012).
- ²R. Fagaly, “Superconducting quantum interference device instruments and applications,” *Review of scientific instruments* **77**, 101101 (2006).
- ³J. Clarke and A. Braginski, “The squid handbook: Applications of squids and squid systems. vol. 2,” (2006).
- ⁴P. Seidel, *Applied Superconductivity: Handbook on Devices and Applications* (John Wiley & Sons, 2015).
- ⁵J. Clarke, Y.-H. Lee, and J. Schneiderman, “Focus on squids in biomagnetism,” *Superconductor Sci. Technol.* **31**, 080201 (2018).
- ⁶C. Granata and A. Vettoliere, “Nano superconducting quantum interference device: A powerful tool for nanoscale investigations,” *Phys. Rep.* **614**, 1–69 (2016).
- ⁷H. Hilgenkamp and J. Mannhart, “Grain boundaries in high- T_c superconductors,” *Reviews of Modern Physics* **74**, 485 (2002).
- ⁸D. Koelle, R. Kleiner, F. Ludwig, E. Dantsker, and J. Clarke, “High-transition-temperature superconducting quantum interference devices,” *Reviews of Modern Physics* **71**, 631 (1999).
- ⁹M. J. Martínez-Pérez and D. Koelle, “Nanosquids: Basics & recent advances,” *Phys. Sci. Rev.* **2** (2016).
- ¹⁰F. Tafuri and J. R. Kirtley, “Weak links in high critical temperature superconductors,” *Reports on Progress in Physics* **68**, 2573 (2005).
- ¹¹E. Y. Cho, Y. W. Zhou, J. Y. Cho, and S. A. Cybart, “Superconducting nano Josephson junctions patterned with a focused helium ion beam,” *Applied Physics Letters* **113**, 022604 (2018).
- ¹²M. Faley, D. Meertens, U. Poppe, and R. Dunin-Borkowski, “Graphoepitaxial high- T_c squids,” in *Journal of Physics: Conference Series*, Vol. 507 (IOP Publishing, 2014) p. 042009.
- ¹³E. Mitchell and C. Foley, “Ybco step-edge junctions with high $I_{c,n}$,” *Supercond. Sci. Technol.* **23**, 065007 (2010).
- ¹⁴F. Öisjöen, J. F. Schneiderman, G. Figueras, M. Chukharkin, A. Kalabukhov, A. Hedström, M. Elam, and D. Winkler, “High- T_c superconducting quantum interference device recordings of spontaneous brain activity: Towards high- T_c magnetoencephalography,” *Appl. Phys. Lett.* **100**, 132601 (2012).

- ¹⁵J. Nagel, K. Konovalenko, M. Kemmler, M. Turad, R. Werner, E. Kleisz, S. Menzel, R. Klingeler, B. Büchner, R. Kleiner, *et al.*, “Resistively shunted $\text{yba}_2\text{cu}_3\text{o}_7$ grain boundary junctions and low-noise squids patterned by a focused ion beam down to 80 nm linewidth,” *Superconductor Science and Technology* **24**, 015015 (2010).
- ¹⁶J. Beyer, D. Drung, F. Ludwig, T. Minotani, and K. Enpuku, “Low-noise $\text{yba}_2\text{cu}_3\text{o}_7$ -x single layer dc superconducting quantum interference device (squid) magnetometer based on bicrystal junctions with 30° misorientation angle,” *Applied physics letters* **72**, 203–205 (1998).
- ¹⁷C. Foley, “Fabrication and characterisation of ybco single grain boundary step edge junctions,” *IEEE Trans. Appl. Supercond.* **9**, 4281–4284 (1999).
- ¹⁸E. Tralbaldo, C. Pfeiffer, E. Andersson, R. Arpaia, A. Kalaboukhov, D. Winkler, F. Lombardi, and T. Bauch, “Grooved dayem nanobridges as building blocks of high-performance $\text{yba}_2\text{cu}_3\text{o}_{7-\delta}$ squid magnetometers,” *Nano letters* **19**, 1902–1907 (2019).
- ¹⁹R. Arpaia, E. Andersson, E. Tralbaldo, T. Bauch, and F. Lombardi, “Probing the phase diagram of cuprates with $\text{yba}_2\text{cu}_3\text{o}_{7-\delta}$ thin films and nanowires,” *Phys. Rev. Mater.* **2**, 024804 (2018).
- ²⁰R. Baghdadi, R. Arpaia, T. Bauch, and F. Lombardi, “Toward $\text{yba}_2\text{cu}_3\text{o}_{7-\delta}$ nanoscale structures for hybrid devices,” *IEEE Trans. Appl. Supercond.* **25**, 1100104 (2015).
- ²¹S. Nawaz, R. Arpaia, T. Bauch, and F. Lombardi, “Approaching the theoretical depairing current in $\text{yba}_2\text{cu}_3\text{o}_7$ -x nanowires,” *Physica C Supercond* **495**, 33–38 (2013).
- ²²R. Arpaia, M. Arzeo, R. Baghdadi, E. Tralbaldo, F. Lombardi, and T. Bauch, “Improved noise performance of ultrathin ybco dayem bridge nanosquids,” *Supercond. Sci. Technol.* **30**, 014008 (2016).
- ²³E. Tralbaldo, M. Arzeo, R. Arpaia, R. Baghdadi, E. Andersson, F. Lombardi, and T. Bauch, “Noise properties of ybco nanostructures,” *IEEE Trans. Appl. Supercond.* **27** (2017).
- ²⁴D. M. Manos and D. L. Flamm, *Plasma etching: an introduction* (Elsevier, 1989).
- ²⁵R. Baghdadi, R. Arpaia, S. Charpentier, D. Golubev, T. Bauch, and F. Lombardi, “Fabricating nanogaps in $\text{yba}_2\text{cu}_3\text{o}_{7-\delta}$ for hybrid proximity-based josephson junctions,” *Physical Review Applied* **4**, 014022 (2015).
- ²⁶C. Granata, A. Vettoliere, R. Russo, M. Fretto, N. De Leo, and V. Lacquaniti, “Three-dimensional spin nanosensor based on reliable tunnel josephson nano-junctions for nanomagnetism investigations,” *Appl. Phys. Lett.* **103**, 102602 (2013).
- ²⁷M. Xie, M. Chukharkin, S. Ruffieux, J. Schneiderman, A. Kalabukhov, M. Arzeo, T. Bauch, F. Lombardi, and D. Winkler, “Improved coupling of nanowire-based high- T_c squid magne-

- tometers—simulations and experiments,” *Supercond. Sci. Tech.* **30**, 115014 (2017).
- ²⁸C. D. Tesche and J. Clarke, “dc squid: Noise and optimization,” *Journal of Low Temperature Physics* **29**, 301–331 (1977).
- ²⁹R. Arpaia, M. Arzeo, S. Nawaz, S. Charpentier, F. Lombardi, and T. Bauch, “Ultra low noise $\text{yba}_2\text{cu}_3\text{o}_{7-\delta}$ nano superconducting quantum interference devices implementing nanowires,” *Appl. Phys. Lett.* **104**, 072603 (2014).
- ³⁰J. Bardeen, “Critical fields and currents in superconductors,” *Reviews of modern physics* **34**, 667 (1962).
- ³¹R. Arpaia, D. Golubev, R. Baghdadi, R. Ciancio, G. Dražić, P. Orgiani, D. Montemurro, T. Bauch, and F. Lombardi, “Transport properties of ultrathin $\text{yba}_2\text{cu}_3\text{o}_{7-\delta}$ nanowires: A route to single-photon detection,” *Physical Review B* **96**, 064525 (2017).
- ³²M. Beasley, J. Mooij, and T. Orlando, “Possibility of vortex-antivortex pair dissociation in two-dimensional superconductors,” *Physical Review Letters* **42**, 1165 (1979).
- ³³H. Bartolf, A. Engel, A. Schilling, K. Il’In, M. Siegel, H.-W. Hübers, and A. Semenov, “Current-assisted thermally activated flux liberation in ultrathin nanopatterned nbn superconducting meander structures,” *Physical Review B* **81**, 024502 (2010).
- ³⁴R. Arpaia, D. Golubev, R. Baghdadi, M. Arzeo, G. Kunakova, S. Charpentier, S. Nawaz, F. Lombardi, and T. Bauch, “Resistive state triggered by vortex entry in $\text{yba}_2\text{cu}_3\text{o}_{7-\delta}$ nanostructures,” *Physica C: Superconductivity and its Applications* **506**, 165–168 (2014).
- ³⁵M. Arzeo, R. Arpaia, R. Baghdadi, F. Lombardi, and T. Bauch, “Toward ultra high magnetic field sensitivity $\text{yba}_2\text{cu}_3\text{o}_{7-\delta}$ nanowire based superconducting quantum interference devices,” *J. Appl. Phys.* **119**, 174501 (2016).
- ³⁶J. Johansson, K. Cedergren, T. Bauch, and F. Lombardi, “Properties of inductance and magnetic penetration depth in (103)-oriented $\text{yba}_2\text{cu}_3\text{o}_{7-\delta}$ thin films,” *Phys. Rev. B* **79**, 214513 (2009).
- ³⁷Magnicon, *SQUID electronics SEL-1*, <http://www.magnicon.com>.
- ³⁸S. Ruffieux, A. Kalaboukhov, M. Xie, M. Chukharkin, C. Pfeiffer, S. Sepehri, J. F. Schneiderman, and D. Winkler, “The role of kinetic inductance on the performance of ybcO squid magnetometers,” *Superconductor Science and Technology* **33**, 025007 (2020).
- ³⁹M. Faley, J. Dammers, Y. Maslennikov, J. Schneiderman, D. Winkler, V. Koshelets, N. Shah, and R. Dunin-Borkowski, “High- T_c squid biomagnetometers,” *Superconductor Science and Technology* **30**, 083001 (2017).
- ⁴⁰M. Chukharkin, A. Kalaboukhov, J. F. Schneiderman, F. Öisjöen, M. Jönsson, M. Xie, O. V.

Snigirev, and D. Winkler, “Improvement of ultra-low field magnetic resonance recordings with a multilayer flux-transformer-based high- T_c squid magnetometer,” *IEEE Trans. Appl. Supercond.* **23** (2013).

⁴¹L. Lee, J. Longo, V. Vinetskiy, and R. Cantor, “Low-noise $\text{YBa}_2\text{Cu}_3\text{O}_{7-\delta}$ direct-current superconducting quantum interference device magnetometer with direct signal injection,” *Applied physics letters* **66**, 1539–1541 (1995).

⁴²B. Riaz, C. Pfeiffer, and J. F. Schneiderman, “Evaluation of realistic layouts for next generation on-scalp meg: spatial information density maps,” *Sci. Rep.* **7**, 6974 (2017).